

$1/x$ Probability Distribution in a Close Proximity of the Bak–Tang–Wiesenfeld Sandpile

A. Shapoval^{1,2,3,*}, B. Shapoval⁴, and M. Shnirman^{3,2}

¹University of Nova Gorica, Nova Gorica, Slovenia

²HSE University, Moscow, Russia

³Institute of Earthquake Prediction Theory RAS, Moscow Russia

⁴University of Colorado Boulder, USA

*corresponding author: abshapoval@gmail.com

February 21, 2022

Abstract

The mechanism of self-organized criticality is based on a steady slow loading and a quick huge stress-release. We add the clustering of the events in space and time to the Bak–Tang–Wiesenfeld cellular automaton and obtain the truncated $1/x$ probability distribution of the events over their sizes.

Keywords: self-organized criticality, scale-free probability distribution, Bak–Tang–Wiesenfeld sandpile

1 Introduction

Introducing the phenomenon of self-organized criticality (SOC) and proposing its explanation with a simple cellular automaton, Bak, Tang, and Wiesenfeld (BTW) wrote “we believe that the new concept of self-organized criticality can be taken much further and might be *the* underlying concept for

temporal and spatial scaling in a wide class of dissipative systems with extended degrees of freedom” [3]. Researchers relate SOC to the property of a system to evolve into a critical state without tuning any parameter. The critical state is associated with the power-laws exhibited by the system. The absence of adjustable parameters such as the temperature or magnetization distinguishes the SOC systems from the systems which generate the critical dynamics at the phase transition. The existence of SOC in the original model is provided for by a BTW mechanism characterized by steady slow loading, the conservative transport of stress from the overloaded locations, and the quick stress-release at the system boundary [5].

The expectations of BTW came true. Examples of SOC were claimed to discover in such different real systems and processes as earthquake formation, forest fires, armed conflicts, the functioning of brains, and the development of cities [2, 15]. The underlying systems exhibit power-law probability distributions of the events over their sizes without external adjustments. Nevertheless, the power-law exponents usually depend on the features of sub-systems (f. .e., seismic faults, geographical regions, and stellar types in the cases of earthquakes, forest fires, and stellar flares, respectively, [13, 1]), thus leaving the question regarding the extent to which the underlying systems are self-organized to be open.

Modeling of real-life systems characterized by power-laws at the critical state can be potentially performed with modifications of the original BTW model that involve various ways of stress propagation including its directed transportation and quenched disorder [7, 11] and implement the BTW mechanism on different spaces including fractals and networks [12, 9, 18, 20]. The value of the exponent τ characterizing the power-law segment $x^{-\tau}$ of the size-frequency relationship has been obtained numerically for various models; rigorous proofs have been obtained for some of them [6].

Changes in the details of the steady loading or transport mechanism conserve the exponent $\tau \approx 1.20$, known [16] for the BTW sandpile, for its deterministic isotropic modifications [4]. A turn to stochastic transport in isotropic sandpiles switches the exponent to $\tau \approx 1.27$ [14, 4, 17]. the nature of self-organized criticality is captured by the independence of the power-laws on model details and the existence of just a few exponents within a broad class of isotropic sandpiles on the square lattice. This imposing feature of the isotropic sandpiles, nevertheless, reduces the range of its direct applications to real systems because the latter exhibit various power-law exponents.

The purpose of this paper is a BTW-mechanism extension that allows

to tune the power-law exponent and belongs to a “narrow neighborhood” of the original BTW sandpile, thus compromising between a certain refusal from self-organization and keeping the mechanism staying behind it. With applications in mind, we weaken two following idealizations of the BTW mechanism: the complete separation of the slow and quick times scales and, as a consequence, the impossibility to combine close in space and time events into mega-events. Our design of the isotropic BTW mechanism on the square lattice will lead to $\sim 1/x$ size-frequency relationship.

2 Model and Results

Definitions. As in the original BTW model, we define the model dynamics on a square lattice. The cells of the lattice are numbered from 1 to $A = L^2$, where $L \in \mathbb{N}$ is the lattice length. Each non-boundary cell i shares a common side with 4 adjacent cells. These 4 cells form the set \mathcal{N}_i of the neighbors of the cell i . The boundary cells have 3 or 2 (in the case of the corner cell) neighbors.

For any i an integer h_i is associated with the cell i . This h_i is interpreted as the number of grains in the cell i or as the height of the pile located in i . The set of the grains $\{h_i\}_{i=1}^A$ forms the configuration. A cell i is stable if its height $h_i < H$, where H is a threshold. The configuration $\{h_i\}_{i=1}^A$ is stable if all the cells are stable. The dynamics are given by changes from one stable configuration to another according to the following procedure.

Avalanches and their size. At each time moment $N = N_L$ different cells i_1, \dots, i_N are chosen at random. Their heights are increased by 1:

$$h_i \longrightarrow h_i + 1, \quad \forall i \in \{i_1, \dots, i_N\}. \quad (1)$$

If none of them attains the threshold H , nothing more occurs at this time moment. If at least a single height attains the threshold H , the grain transport starts: unstable cells pass H grains equally to the neighbors. Formally, for any i with $h_i = H$,

$$h_i \longrightarrow h_i - H \quad (2)$$

$$h_j \longrightarrow h_j + 1 \quad \forall j \in \mathcal{N}_i. \quad (3)$$

Let us say that each unstable cell generates an avalanche. If n unstable cells $\{i_1, \dots, i_n\}$, $n \leq N$, appear as a result of the grain adding at the time t , then

n avalanches $a_{i_1,t}, \dots, a_{i_n,t}$ occur at t . At the beginning, each avalanche $a_{i_k,t}$, $k = 1, \dots, n$, “propagates” to a single cell, namely, the origin i_k that generates the avalanche. At this moment the size $s_{i_k,t}$ of each avalanche is set to 0. The unstable cells i_1, \dots, i_n and their neighbors update the heights in line with (2), (3) simultaneously. The size $s_{i_k,t}$ of the avalanches $a_{i_k,t}$ is increased from 0 to 1. The updates can induce instability in other cells. New unstable cells are associated with just those avalanches that propagate to them. In other words, if an unstable cell j obtained a grain from a cell j' associated with the avalanche $a_{i,k}$, then j is also associated with $a_{i,k}$. If two (or more) avalanches propagate to j (i. e., pass a grain to j), then the choice of the avalanche to be assigned to j is performed at random. Each update induced by the instability of the cell associated with the avalanche $a_{i_k,t}$ results in the increase of its size $s_{i_k,t}$ by 1, $k = 1, \dots, n$. The updates ruled by (2) and (3) occur while there are unstable cells. As soon as $h_i < H$ for all cells i (i. e., a stable configuration is attained), the next time moment begins.

Note that a cell can attain the threshold H several times within a single time moment. The correspondence to the avalanche is determined when the cell becomes unstable. The result of the determination can differ from case to case.

Mega-avalanches and their size. We note that the above dynamics extends the original BTW model with $N = 1$ to the case of $N > 1$. The extension results in several avalanches spreading simultaneously. Resolving this ambiguity, we merge the avalanches that are close in space and time into the mega-avalanches and focus on the probability distribution of the mega-avalanches. A mega-avalanche consists of a single avalanche if this avalanche is not merged with another avalanche.

In the current version of the model, the merging rule is formulated only with the origin and the size of the avalanches and the time of their observation allowing for random factors to reduce the time of the computer simulation. The proximity between the avalanches is found through the comparison of the Manhattan distance (the sum of the absolute differences of the Cartesian coordinates) ρ with an appropriate function of the avalanches’ sizes.

To formalize the rule, we introduce the characteristic (two-state) function $\mathbf{1}_{\text{condition}} = \mathbf{1}_{\text{condition}}(i_1, t_1, i_2, t_2)$ that attains 1 if the **condition** holds and 0 otherwise. Let $U \sim \mathbf{Uni}(0, 1)$ be a uniform $[0, 1]$ random variable. Then the

inequality

$$\mathbf{1}_{\rho(i_1, i_2) < C' L(s_{i_1, t_1}^d + s_{i_2, t_2}^d)} \cdot \mathbf{1}_{|t_1 - t_2| \leq T} + \mathbf{1}_{U < p} \cdot \mathbf{1}_{t_1 = t_2} > 0 \quad (4)$$

underlies the merging of a_{i_1, t_1} and a_{i_2, t_2} , where $p \in [0, 1]$, $T \geq 0$, $C' > 0$, and $d > 0$ are the parameters. We fix $C' = 0.025$ and $d = 0.33$, taking them from a range of affordable values. The specific choice affects the other parameters that result in the scale-free distribution $f_L(s)$.

The specific choice of the parameters $T = 0$ and $p = 0$ simplifies (4) to

$$\rho(i_1, i_2) < C' L(s_{i_1, t_1}^d + s_{i_2, t_2}^d), \quad t_1 = t_2. \quad (5)$$

The switch to positive values of p admits a random merging of the avalanches. Positive integers T allow to coalesce the avalanches observed at subsequent time moments. As we will see, a gradual increase in T from zero is required rather than the jump to 1. This leads us to the fractional values of $T \in (0, 1)$ and the probabilistic nature of the inequality $|t_1 - t_2| \leq T$. This inequality is claimed to hold with certainty if $t_1 = t_2$ and with probability T if $|t_1 - t_2| = 1$.

If the avalanches $a_{i_1, t_1}, \dots, a_{i_k, t_k}$, $k \geq 1$, form the mega-avalanche a , then the size $s = \text{size}(a)$ of a is the sum of the corresponding sizes: $s = s_{i_1, t_1} + \dots + s_{i_k, t_k}$. The origin of the mega-avalanches is the weighted average of the origins of the contributing avalanches, where the weights are proportional to the sizes of the avalanches.

Probability distribution of the mega-avalanches. Let $f_L(s)$ be the empirical density of the mega-avalanches occurred on the $L \times L$ -lattice with respect to their sizes s and $F_L(s) = \#\{a : \sigma = \text{size}(a) \in [s/\Delta s, s\Delta s]\} / \#\{a : \sigma = \text{size}(a) > 0\}$ be the proportion of the mega-avalanches with the size located between $s/\Delta s$ and $s\Delta s$, where $\Delta s = 1.2$ is chosen in the graphs. Note that the focus on $F_L(s)$ instead of $f_L(s)$ increases the exponent of the power-law from $-\tau$ to $-\tau + 1$, as it follows from the integration:

$$\int_{s/\Delta s}^{s\Delta s} \sigma^{-\tau} d\sigma = \begin{cases} \frac{1}{1-\tau} ((\Delta s)^{1-\tau} - (\Delta s)^{\tau-1}) \cdot s^{1-\tau}, & \text{if } \tau \neq 1, \\ 2 \ln \Delta s \cdot s^0, & \text{if } \tau = 1. \end{cases}$$

We have sampled the data for the empirical functions $f_L(s)$ and $F_L(s)$ for $5 \cdot 10^5$ subsequent time moments for all lattices. Sampling is performed after some transient period to let the system reach the steady state and eliminate

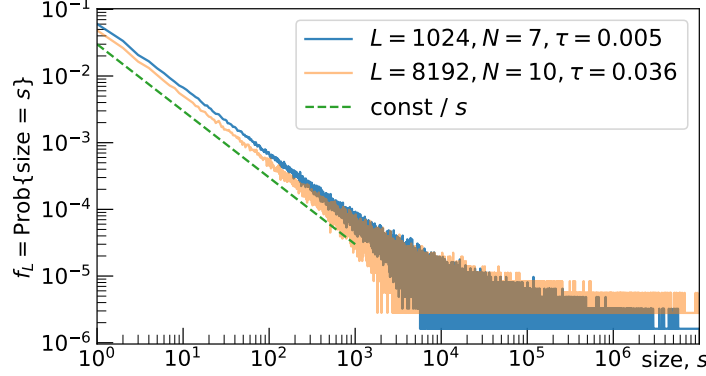


Figure 1: The probability density function $f_L(s)$ of mega-avalanche's sizes; the part with $s > 10^7$ is omitted.

the dependence on the initial conditions. The graph of $f_L(s)$ is too noisy at the right to illustrate the full power-law segment (Figure 1 exhibits $f_L(s)$ found with $L = 1024$ and $L = 8192$). On the contrary, gathering the points of $f_L(s)$ within the exponentially growing bins into $F_L(s)$, we give the relevant pattern of the power-law segment up to the abrupt bend down in the log-log scale, Figure 2. The scaling $s \rightarrow s/L^2$ normalizes the right endpoint of the power-law segment, Figure 2.

All four graphs of Figure 2 follow an almost flat step that is turned to a quick decay at the right. We emphasize that the power-law exponents are found with the maximum likelihood method applied to the empirical probability density $f_L(s)$. These exponents $\tau = \tau_L$ are (very) close to 1. The best fits to $F_L(s)$ with these exponents increased by 1 are shown in Figure 2, where the values $1 - \tau$ are written next to the curves. These values suggest that the graphs are almost flat, which is, indeed, the case.

The power-law segments are collapsed after the transformation of the axis: $s \rightarrow s/L^2$, $F_L \rightarrow F_L \log L$ (Figure 2b). The logarithmic correction of the vertical axis is caused by the proximity of the probability density to $1/s$ -segment, the power-law scaling of the right endpoint s^* of this segment, and a fast decay of F_L at the right from s^* . Then the integration of the density $f_L(s) = C_L/s$ over $[1, +\infty]$ results in the estimate $C_L \cdot c \log L \approx 1$, which implies $C_L \sim 1/\log L$. The fact that the transformation $s \rightarrow s/L^2$ of the horizontal axis normalizing the right endpoint of the power-law segment does

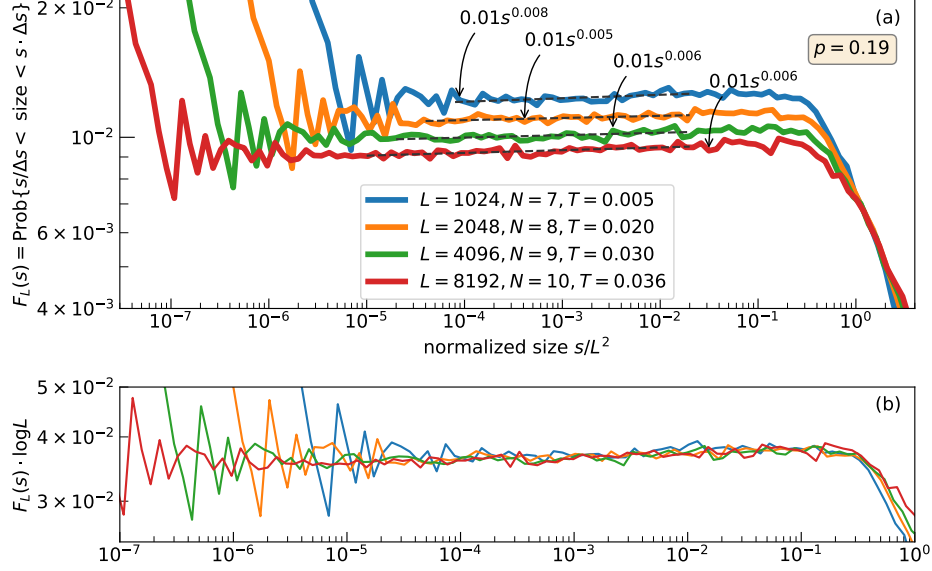


Figure 2: Power-law segment of the probability distributions of avalanches' sizes, where the length of the horizontal bins increases exponentially (which rises the power-law exponent by 1) and the vertical axis is (b) and is not (a) normalized.

not allow to collapse the tails is inherited from the BTW sandpile (because of its multifractal scaling [19]).

The transition from the BTW power-law to approximately $1/s$ truncated probability distribution of the mega-avalanches is performed with the logarithmic extra-loading $N \sim \log L$ and the probabilistic merging of the spatio-temporal clusters of avalanches into the mega-avalanches. The logarithmic extra-loading $N \sim \log L$ itself with deterministic merging defined by (5) conserves the density of the grains at its critical level (not supported by graphs) and creates two power-law parts of $F_L(s)$. The left part extends to the size of approximately 3000 for all values of L (as seen with the blue curve in Figure 3). Without illustration of the dependence on L , we just note that the right endpoint of second power-law part scales as L^2 and its the slope becomes steeper as L increases. The introduction of the time clustering with the parameter $T > 0$ makes the right power-law part flatter in the log-log scale (the orange curve in Figure 3). The contraction of the gap between two consecutive values of T shown in Figure 2 in approximately 1.5 times

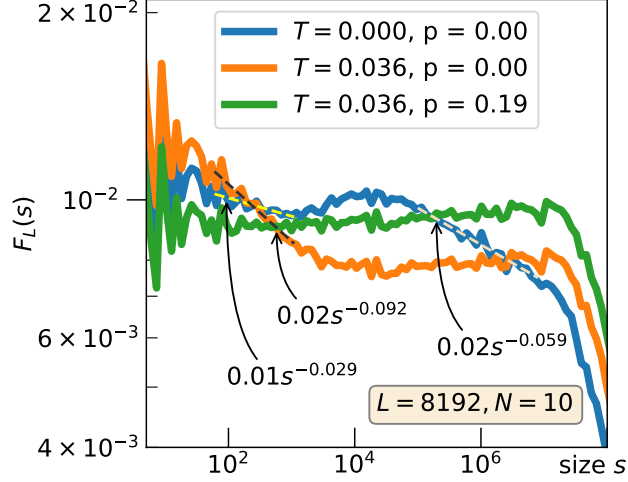


Figure 3: A part of $F_L(s)$ computed with the parameters reported in the legend and $s^{1-\tau}$ -fits.

suggests that T saturates at ≈ 0.05 as $L \rightarrow \infty$. The right power-law part becomes narrow with the decrease of L , disappearing as L falls below 1024 (not supported by graphs). Therefore, T fixed to 0.005 for $L = 1024$ is taken as 0 for $L = 512$ or smaller.

Interestingly, the changes in the exponent of the right power-law part preserves the existence of the power-law at the left but alters its slope. The return to the flat part of $F_L(s)$ is performed with the random merging through the adjustment of the parameter p . The choice of $p = 0.19$ is affordable for all graphs constructed with different values of L . Thus, our merging is expected to lead to $T \approx 0.05$, $p \approx 0.19$, and $N \sim \log L$ as L goes to infinity.

3 Discussion and Conclusion

We insist that our approach principally differs from the two following simple constructions: the summation of the independent power-law random variables and merging of avalanches, which are adjacent in time, in the original BTW model. The first construction leads to the probability density, which is concave in the log-log scale, tending to the power function at the right part of the graph (the grey curve in Figure 4 through 8 convolutions, i. e., the

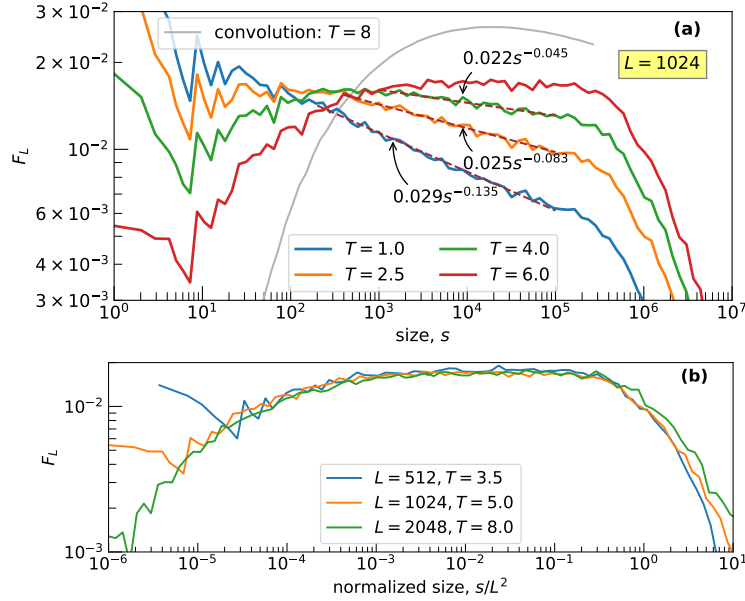


Figure 4: A segment of the probability distributions $F_L(s)$ (summed up over exponentially growing bins) of the sizes of the mega-avalanches obtained through the merging of the avalanches occurred within T consecutive time moments in the classical BTW model. L^2 -normalization of the sizes collapses $F_L(s)$ with adjusted T , (b). The gray curve (in (a)) is obtained through the convolution of 8 probability densities $\sim s^{-1.20}$ with the support $[1, 1024]$.

summation of 8 independent $1/x^{1.20}$ random variables with the support on $[1, 1024]$). The second construction can be defined through the coalescence of avalanches occurred during T subsequent time moments. The uncertainty with fractional values T is resolved with a probabilistic rule (say, if $T = 2.5$ and a_t is not merged with a_{t-1} , then the avalanches a_t , a_{t+1} , and a_{t+2} are combined with certainty, whereas the avalanche a_{t+3} is added with the probability of 0.5). This modification of the BTW model preserves the power-law segment that *does not* extend to the right with the growth of the system. The power-law part of $F_L(s)$ constructed for the different values of L is collapsed after the normalization of the size by the lattice area, Figure 4.

The paper gives evidence that the $1/x$ power-law is feasible with isotropic extensions of the BTW sandpile (Figure 2). The extension is constructed with the stress accumulation, proportional to $\log L$, and the coalescence of

the avalanches propagated closely in space and time. Such a coalescence is known, for example, in seismology, as the stress accumulation and the earthquakes themselves occurred in the slow and quick time respectively are not completely separated [10].

The details of the construction are likely to be designed in various ways. Proposed minor deviations from the BTW model through the parameter domain preserve the critical density of the grains and the power-law size-frequency relationship for the mega-avalanches over the majority of feasible sizes (Figure 3). The adjustment of the parameters pulls the exponent τ towards 1 (through a weak time clustering, parameter T) and corrects the slope of the restricted left part to fit the whole power-law segment (with the random coalescence in space, parameter p). Thus, our approach does not require any tuning of the dissipation-to-loading ratio as in attempts to relate self-organized criticality to the phase transition modeling [8] but controls the universality class of the sandpile and might lead to adjustable power-law exponents in a neighborhood of 1. This would improve our understating of real-life self-organized critical phenomena.

References

- [1] M. J. Aschwanden and M. Güdel. Self-organized criticality in stellar flares. *The Astrophysical Journal*, 910(1):41, 2021.
- [2] P. Bak. *How nature works: the science of self-organized criticality*. Springer Science & Business Media, 2013.
- [3] P. Bak, C. Tang, and K. Wiesenfeld. Self-organized criticality: an explanation of $1/f$ noise. *Phys. Rev. Lett.*, 59:381–383, 1987. doi: 10.1103/PhysRevLett.59.381.
- [4] O. Biham, E. Milshtein, and O. Malcai. Evidence for universality within the classes of deterministic and stochastic sandpile models. *Phys. Rev. E*, 63(6): 061309, 2001.
- [5] P. De Los Rios and Y. Zhang. Universal $1/f$ noise from dissipative self-organized criticality models. *Phys. Rev. Lett.*, 82(3):472, 1999.
- [6] D. Dhar. Theoretical studies of self-organized criticality. *Physica A: Statistical Mechanics and its Applications*, 369(1):29–70, 2006.

- [7] D. Dhar and R. Ramaswamy. Exactly solved model of self-organized critical phenomena. *Phys. Rev. Lett.*, 63(16):1659, 1989.
- [8] R. Dickman, A. Vespignani, and S. Zapperi. Self-organized criticality as an absorbing-state phase transition. *Phys. Rev. E*, 57(5):5095, 1998.
- [9] K.-I. Goh, D.-S. Lee, B. Kahng, and D. Kim. Sandpile on scale-free networks. *Phys. Rev. Lett.*, 91(14):148701, 2003.
- [10] H. Kanamori. Earthquake prediction: An overview. In *International Handbook of Earthquake and Engineering Seismology. International geophysics series*, volume 81B, pages 1205–1216. Academic Press, 2003.
- [11] R. Karmakar, S. Manna, and A. Stella. Precise toppling balance, quenched disorder, and universality for sandpiles. *Phys. Rev. Lett.*, 94(8):088002, 2005.
- [12] B. Kutnjak-Urbanc, S. Zapperi, S. Milošević, and H. Stanley. Sandpile model on the sierpinski gasket fractal. *Phys. Rev. E*, 54(1):272, 1996.
- [13] B. Malamud, G. Morein, and D. Turcotte. Forest fires: an example of self-organized critical behavior. *Science*, 281(5384):1840–1842, 1998.
- [14] S. Manna. Two-state model of self-organized criticality. *Journal of Physics A: Mathematical and General*, 24(7):L363, 1991.
- [15] D. Marković and C. Gros. Power laws and self-organized criticality in theory and nature. *Physics Reports*, 536(2):41–74, 2014.
- [16] V. Priezzhev, D. Ktitarov, and E. Ivashkevich. Formation of avalanches and critical exponents in an abelian sandpile model. *Phys. Rev. Lett.*, 76(12):2093, 1996.
- [17] A. Shapoval and M. Shnirman. Crossover phenomenon and universality: From random walk to deterministic sand-piles through random sand-piles. *International Journal of Modern Physics C*, 16(12):1893–1907, 2005.
- [18] A. Shapoval and M. Shnirman. The BTW mechanism on a self-similar image of a square: A path to unexpected exponents. *Physica A: Statistical Mechanics and its Applications*, 391(1-2):15–20, 2012.
- [19] C. Tebaldi, M. De Menech, and A. L. Stella. Multifractal scaling in the bak-tang-wiesenfeld sandpile and edge events. *Phys. Rev. Lett.*, 83(19):3952, 1999.

- [20] N. Zachariou, P. Expert, M. Takayasu, and K. Christensen. Generalised sand-pile dynamics on artificial and real-world directed networks. *PloS One*, 10(11):e0142685, 2015.